## Mapping urban heat islands in Pune, India: ecological impacts and environmental challenges

ARTICLE TEMPLATE

# Mapping Urban Heat Islands in Pune, India: Ecological Impacts and Environmental Challenges

Aditya Raj[a] , A. Anjali[a], Vishal Krishna Singh[b], and Vijay Bhaskar Semwal [c]

[a]Department of Information Technology, ABV-Indian Institute of Information Technology and Management Gwalior
[b] School of Computer Science and Electronic Engineering, University of Essex, U.K.
[c] Dept. of Computer Science and Engineering, Maulana Azad National Institute of Technology, Bhopal.

**ARTICLE HISTORY**
Compiled March 18, 2025

**ABSTRACT**
Heat waves increasingly affect cities, amplifying the urban heat island (UHI) effect, often measured through land surface temperature (LST). In Pune, India, rapid urbanization between 2013 and 2022 has driven significant land use and land cover (LULC) changes, with a staggering 89.24% increase in built-up areas and a decline of 991.4 km² in vegetation cover. Using satellite remote sensing data processed via Google Earth Engine, this study reveals a pronounced rise in LST, with mean temperatures increasing from 27°C in 2013 to 36°C by 2022, and a notable expansion in regions experiencing temperatures between 25°C and 32°C. Additionally, $NO_2$ levels slightly rose, further stressing environmental conditions. Central Pune was identified as a high-risk zone for adverse climatic impacts, emphasizing the urgent need for ecological conservation, climate adaptation, and sustainable urban planning to mitigate the growing UHI effect amidst accelerating urbanization in Indian cities.

**KEYWORDS**
Urban heat island, Land surface temperature, Land use land cover, Remote sensing, Geospatial analysis, Vegetation indices, Air pollution, Microclimate,

## 1. Introduction

Urbanization has profoundly transformed land use and land cover (LULC), replacing natural vegetation with impervious surfaces like roads, buildings, and infrastructure (Guo et al. 2024; Chauhan and Jethoo 2023). This transformation induces the urban heat island (UHI) effect, characterized by elevated temperatures in urban areas compared to rural surroundings. Key contributors include heat absorption by urban materials, waste heat emissions, and reduced vegetation cover, exacerbating environmental and public health challenges (Elmarakby and Elkadi 2024). As urban expansion accelerates, assessing UHI formation is essential for climate-resilient urban planning. Rapid urbanization in South Asia, with nearly 50% of India's population projected to reside in urban areas by 2050 (National-Commission-on-Population-Report), intensifies UHI effects. Urbanization-driven changes disrupt local microclimates, increase energy demands, and degrade air quality (Bagyaraj et al. 2023) (Badugu et al. 2023). Factors

Contact A. Anjali at email: anjali@iiitm.ac.in, Corresponding Author

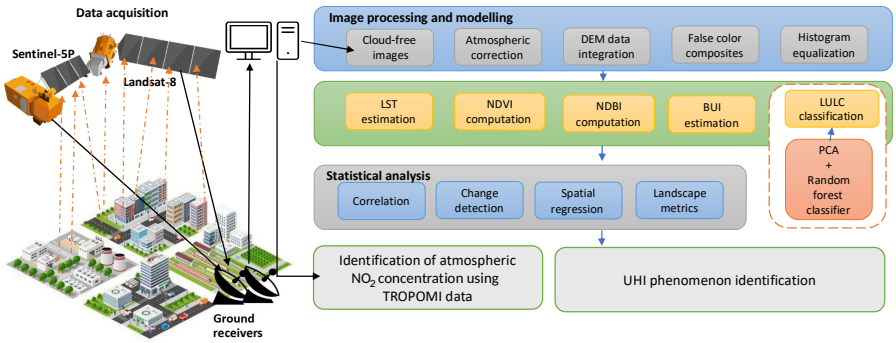


Figure 1.: Proposed Methodology for identification UHI Phenomenon

such as anthropogenic heat emissions, limited evapotranspiration, and socioeconomic activities, including industrial zones and transportation hubs, further exacerbate UHI impacts (Firozjaei et al. 2019; Wang et al. 2020; Portela et al. 2020; Mohammad and Goswami 2022). Green infrastructure offers sustainable solutions to mitigate UHI effects by enhancing shading, evapotranspiration, and albedo (Wu et al. 2024). Properly planned urban green spaces balance thermal regulation, ecological benefits, and air quality improvement (Bagyaraj et al. 2023). Remote sensing and geographic information systems (GIS) enable effective monitoring of LULC changes, extraction of indices like Normalized Difference Vegetation Index (NDVI), Normalized Difference Built-up Index (NDBI), and assessment of thermal and pollution dynamics (Kowe et al. 2022; Harod and Rajasekaran 2024).

This study leverages satellite remote sensing to examine UHI dynamics in Pune, India, from 2013-2022. It analyzes LULC changes and their impacts on land surface temperature (LST), NDVI, NDBI, and Nitrogen Dioxide ($NO_2$) concentrations, identifying UHI risk zones and assessing urbanization's environmental implications. The findings underscore the importance of evidence-based urban planning and climate resilience. Satellite-based tools, such as Landsat and Sentinel-5P, provide critical data for monitoring surface characteristics, measuring LST, and linking air quality to UHI effects (Kowe et al. 2022; Harod and Rajasekaran 2024). Unlike existing works that often focus on individual parameters, we provide a comprehensive approach to understand the synergistic effects of urbanization and vegetation decline on rising temperatures. While this study focuses on horizontal dimensions of urban morphology, such as LULC changes, vertical structures like building heights are excluded due to dataset limitations. Future research incorporating three-dimensional urban morphology is recommended to comprehensively understand UHI dynamics.

## 2. Materials and Methods

### 2.1. *Materials*

#### *2.1.1. Landsat-8 Data and TROPOMI Data*

Landsat 8 OLI and TIRS data, acquired from Google Earth Engine (Landsat-8 C2 Level-2), provided thermal data (Band 10, 100 m resolution) and surface reflectance (15–30 m resolution). Images with <10% cloud cover were selected to ensure reliabil-

ity, focusing on LST variations rather than absolute values (Portela et al. 2020). The TROPOMI sensor on the Sentinel-5P satellite measures atmospheric $NO_2$ concentrations with high precision. Its improved spatial resolution (3.5–5.5 km post-2019) and high signal-to-noise ratio enable effective monitoring of sunlight reflection and $NO_2$ levels (Ialongo et al. 2020).

#### *2.1.2. Population Distribution*

Pune, a rapidly urbanizing city in Maharashtra, India, has experienced steady population growth, peaking at 2.99% annually until 2018 and reducing to 2.63% by 2022 (Karutz et al. 2023). This growth has reshaped land use patterns, increasing surface temperatures and driving urbanization over the past two decades.

### 2.2. *Study Area*

Pune, situated at 18.5204° N, 73.8567° E on the Deccan Plateau at 560 m, is a rapidly urbanizing IT and automotive hub. The city has a semi-arid climate with hot summers, monsoons (June–September), and mild winters.

### 2.3. *Data Preprocessing*

Landsat 8 OLI data (30 m resolution) from 2013–2022 were processed via Google Earth Engine (GEE). Cloud-free images from the same season ensured temporal consistency. Atmospheric correction removed artifacts, histogram equalization enhanced contrast, and Principal Component Analysis (PCA) reduced dimensionality, retaining key spectral features.

### 2.4. *Experimental Design*

The proposed methodology (Figure 1) processed datasets in GEE to generate false-color composites (FCC) for the study area. Key indices, including NDVI, Built-up Index (BUI), and LST, were calculated to identify Urban Heat Island areas. Supervised classification categorized land cover into urban areas, vegetation, water bodies, and barren land, enabling detailed spatial analysis of UHI dynamics. Change detection analysis compared classified land cover maps, NDVI, and LST distributions from 2013 to 2022, revealing urbanization trends and thermal environment impacts. Landscape Metrics quantified patterns, connectivity, and fragmentation, complementing the ecological assessment. Statistical analyses, including spatial regression and Landscape Metrics calculations, were performed in R, while ArcGIS 10.8 generated spatial maps for land cover, UHI intensity, and ecological evaluations.

### 2.5. *Land Use and Cover Change (LUCC) Calculation*

A hybrid approach combining Random Forest (RF) and PCA improved LUC classification accuracy. Five scenes of Landsat-8 OLI images (2013–22) were processed. The RF algorithm classified spectral images, while PCA reduced dimensionality, extracting key features for input to the RF classifier. The combination provided precise LUC classification, facilitating analysis of urban dynamics. The PCA analysis and classification algorithm are presented below, and the notations are described in a footnote.

PCA Analysis and Classification

**Input:** Composite image data $\mathbf{X}$
**Output:** Classified result using Random Forest
**Step 1:** Select spectral bands from the composite image.
**Step 2:** Centre the data:
$\mathbf{X}_{\text{centred}} \leftarrow \mathbf{X} - \frac{1}{n}\sum_{i=1}^{n}\mathbf{X}_i$ {where $n$ is the number of data points}
**Step 3:** Compute the covariance matrix:
$\mathbf{C} \leftarrow \frac{1}{n-1}\mathbf{X}_{\text{centred}}^{T}\mathbf{X}_{\text{centred}}$
**Step 4:** Perform eigen analysis to obtain eigenvalues and eigenvectors:
$\mathbf{C}\boldsymbol{V} = \lambda\boldsymbol{V}$ {where $\boldsymbol{V}$ represents the eigenvectors and $\lambda$ the eigenvalues}
**Step 5:** Sort eigenvalues in descending order and select the top $k$ principal components.
**Step 6:** Transform the data using the selected eigenvectors:
$\mathbf{X}_{\text{PCA}} \leftarrow \mathbf{X}_{\text{centred}}\boldsymbol{V}_k$
**Step 7:** Apply Random Forest classifier:
Classified $\leftarrow RF(\mathbf{X}_{\text{PCA}})$
**Step 8:** Validate classification performance using the kappa coefficient:
$P_0 \leftarrow \sum_{i=1}^{r}(P_{i+} \cdot P_{+j})$
$P_c \leftarrow \sum_{i=1}^{r}(P_{i+} \cdot P_{+j})$
$K_\lambda \leftarrow \frac{P_0 - P_c}{1 - P_c} = 0$

**Notation:** $\mathbf{X}_{\text{centred}}$: Centred data matrix obtained by subtracting the mean. $\mathbf{X}$: Original data matrix. $n$: Number of data points. $\mathbf{C}$: Covariance matrix computed from centred data. $\boldsymbol{V}$: Eigenvectors representing principal components. $\lambda$: Eigenvalues corresponding to the eigenvectors. $\boldsymbol{V}_k$: Top $k$ selected principal components. $\mathbf{X}_{\text{PCA}}$: Transformed data after applying PCA. $RF$: Random Forest classifier. $P_0$: Proportion of observed agreement. $P_c$: Proportion of chance agreement. $r$: Number of rows in the error matrix. $P_{i+}$, $P_{+j}$: Marginal totals for rows and columns in the error matrix. $K_\lambda$: Kappa coefficient, measuring classification accuracy.

### 2.5.1. *Mapping UHI, Non-UHI, and UHS*

The conventional method quantifies UHIs by assessing the temperature difference between urban and rural areas. UHIs were identified as regions where the LST exceeded the mean rural LST:

$$\text{UHI} = \text{LST}_{\text{urban}} - \text{LST}_{\text{rural}}. \tag{1}$$

This method provides a straightforward assessment of heat intensity influenced by land cover. Additionally, Urban Heat Stress (UHS) areas, indicative of extreme temperature conditions, were identified using a higher threshold based on statistical deviation (Wang et al. 2020):

$$\text{LST} > \mu + 2 \times \delta. \tag{2}$$

where $\mu$ and $\delta$ denote the mean and standard deviation of LST, respectively.

### 2.5.2. *Urban Thermal Field Variance Index (UTFVI)*

UTFVI quantifies UHI intensity using multi-temporal LST data. Key meteorological factors, such as temperature, wind speed, and precipitation, were considered for consistency across dates. The UTFVI (Portela et al. 2020; Mohammad and Goswami 2022) is calculated as:

$$\text{UTFVI} = \frac{T_s - T_{\text{mean}}}{T_{\text{mean}}}, \tag{3}$$

where $T_s$ is the LST at a specific location, and $T_{\text{mean}}$ is the regional mean LST. This index informs urban planning and environmental management by quantifying thermal variations.

### 2.5.3. *Calculation of $NO_2$ Concentration*

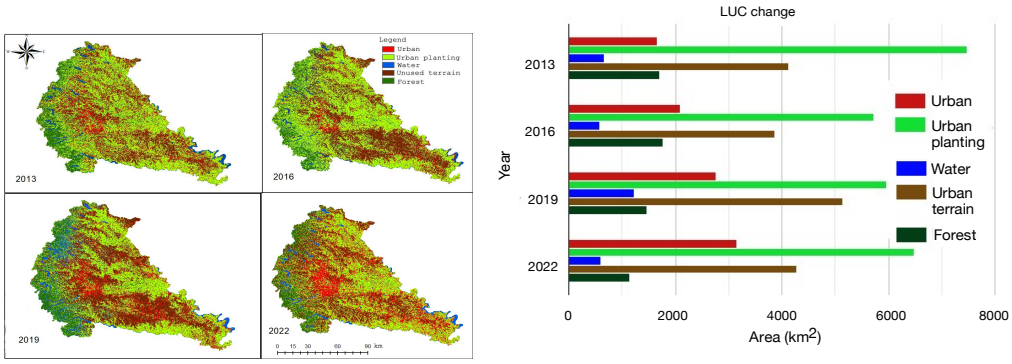


(a) (b)

Figure 2.: (a) LUCC changes over the study period (b) LUC changes over the study period.

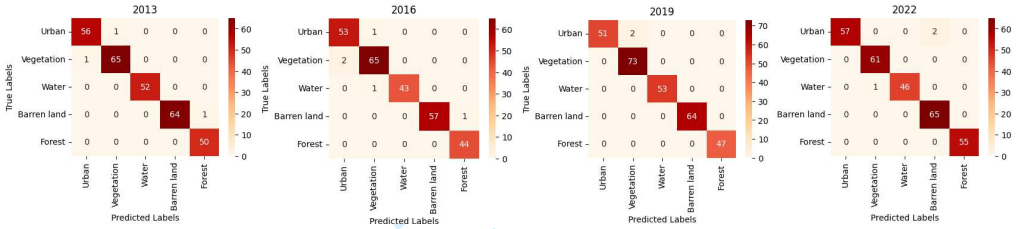


Figure 3.: LULC Confusion Matrices over Study Years

TROPOMI $NO_2$ data for 2020 and 2023 were analyzed with cloud masking to ensure accuracy. A median composite from May 2022 was used, and the mean concentration of $NO_2$ was calculated as the mean vertical column density of the tropospheric $NO_2$. Furthermore, a time series analysis was conducted to examine the relationship between the day of the year (DOY) and the mean $NO_2$ concentration, highlighting seasonal variations in pollution levels. This analysis provides insights into long-term trends, helping to understand how $NO_2$ levels fluctuate over time and their correlation with urbanization.

## 3. Experimental Results

### 3.1. *LUC Classification*

Pune's land use and cover (LUC) maps were presented in Figure 2a for 2013, 2016, 2019, and 2022, classifying six categories: water, vegetation, forest, urban, unused terrain, and cropland. Figure 2b shows water bodies shrank from 673.7 $km^2$ in 2013 to 595.5 $km^2$ in 2022, a decline of 78.2 $km^2$. Vegetation cover decreased from 7473.5 $km^2$ to 6482.1 $km^2$, a 991.4 $km^2$ loss which can be observed in Figure 2b. Moreover, Figure 2b highlighted forested areas were reduced by 562 $km^2$, while wasteland increased by 147.1 $km^2$. Cropland also witnessed a significant decline. Figure 2a and Figure 2b show that urban areas expanded significantly, from 1663.4 $km^2$ in 2013 to 3147.9 $km^2$ in 2022, marking an 89.24% growth over ten years. To evaluate the accuracy of the LUC classification, confusion matrices were generated for 2013, 2016, 2019, and 2022,

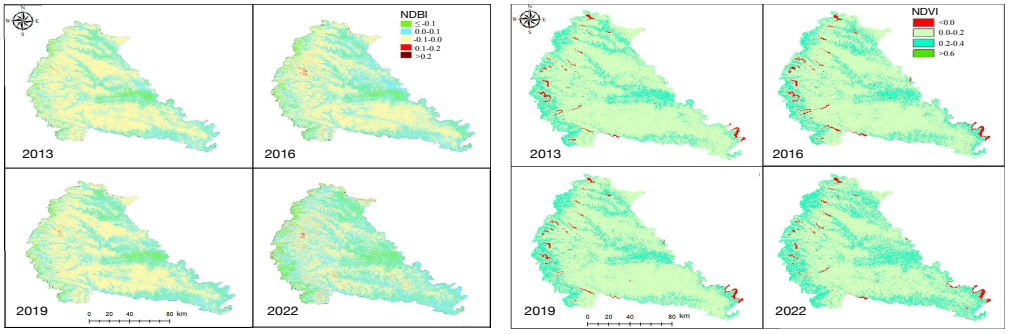


(a) (b)

Figure 4.: (a) NDBI changes over the study period. (b) NDVI changes over the study period.

Table 1.: LUCC Evaluation Metrics

| Year | Accuracy | Kappa Coefficient |
|---|---|---|
| **2013** | 0.993 | 0.991 |
| **2016** | 0.977 | 0.971 |
| **2019** | 0.993 | 0.991 |
| **2022** | 0.989 | 0.986 |

Table 2.: Average NDVI and NDBI values

| Year | Average NDBI | Average NDVI |
|---|---|---|
| **2013** | -0.0005 | 0.133 |
| **2016** | 0.0028 | 0.135 |
| **2019** | -0.0008 | 0.135 |
| **2022** | -0.004 | 0.152 |

Table 3.: Min and Max LST values (°C)

| Year | Min LST | Max LST |
|---|---|---|
| **2013** | 18.2 | 54 |
| **2016** | 18.1 | 54 |
| **2019** | 27.4 | 53.3 |
| **2022** | 17.1 | 53.1 |

as shown in Figure 3. The overall classification accuracies and corresponding Kappa coefficients for each year are summarized in Table 1.

### 3.2. *Normalized Difference Vegetation Index and Built-Up Index*

The NDVI values in Figure 4b and Table 2 showed an upward trend from 0.133 in 2013 to 0.152 in 2022, indicating increased vegetation density. NDVI is essential for assessing UHI effects, as vegetation aids microclimate regulation through shading and evapotranspiration. Its rise may result from afforestation, urban greening, or land use changes, influencing thermal dynamics. Analyzed alongside LST and NDBI, it helps evaluate urban temperature variations. Meanwhile, NDBI remained stable, reflecting minimal land cover changes (Figure 4a, Table 2).

### 3.3. *Land Surface Temperature Calculation*

The LST analysis for Pune from 2013 to 2022 reveals a significant warming trend, with the mean LST increasing from 27.7 °C to 36.8 °C (Figure 5a). Over time, areas with lower temperatures (17–25°C) shrank, while regions with higher temperature ranges (32–40°C and 40–48°C) expanded significantly, indicating increased heat intensity. The minimum LST ranged from 17.1 °C to 27.4 °C, while the maximum LST remained stable in a range of 53.1 - 54.0 °C (Table 3 and Figure 5b).

In addition, a trend analysis for 2013 to 2022 is presented in Figure 6a, indicating a decrease in the coverage of the non-UHI area, accompanied by an increase in the extent of the UHI and LST values, emphasizing the ecological impact of urban expansion on temperature and vegetation patterns. Furthermore, a heat map presented in Figure

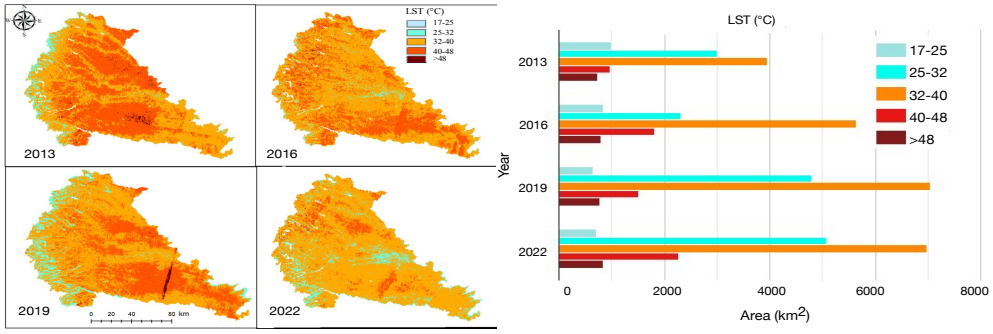


(a) (b)

Figure 5.: (a) Spatiotemporal Variation in LST (2013-2022). (b) Temperature distribution across categories.

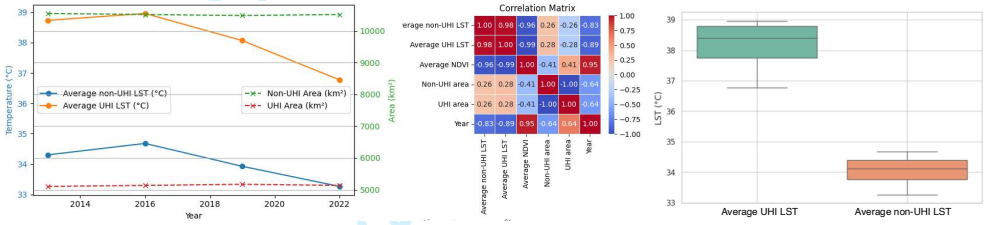


Figure 6.: (a) Temporal Trends in LST, UHI, non- UHI and Area Extents (b) Correlation Heatmap of Key Variables (c) Box plot Comparison of LST in UHI vs. Non-UHI Areas

6b of the correlation coefficients demonstrates a strong negative relationship between the extent of the NDVI and the UHI area, linking the loss of vegetation with rising temperatures. Finally, a box plot comparison of UHI and non-UHI areas shows consistently higher LST values in UHI regions, highlighting urbanization's role in localized warming in Figure 6c.

### 3.4. *Spatial Distribution of UHI and Non-UHI*

Figure 7a depicts the consistent expansion of UHI-affected areas in Pune from 2013 to 2022, initially spanning from the southwest to the northeast. By 2022, these regions encompassed the city's southwest, east, and central core. Non-UHI temperature thresholds were recorded as 19.10°C (2013), 18.95°C (2016), 28.60°C (2019), and 31.47°C (2022). UHI intensity varied due to land use changes, urbanization, and climate shifts, affecting impermeable surfaces, green spaces, and localized microclimates. Furthermore, the transect in Figure 7a represents the progressive changes in temperature thresholds throughout Pune, which are plotted in the inset graph, and shows the spatial spread of UHI-affected areas over time. Additionally, Figure 7b shows the highest UHI intensity was observed in 2022 (0.72°C), while the lowest was in 2016 (0.11°C). Moreover, the transects in Figure 7b have been plotted to depict variations in UHI intensity, emphasizing temperature differences between UHI and non-UHI zones.

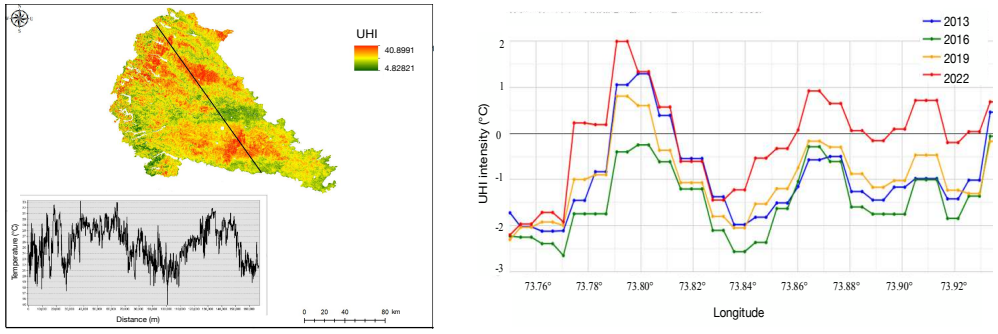


(a) (b)

Figure 7.: (a) UHI Intensity Map of Pune (2022). (b) UHI Profile along Transect (2013–2022).

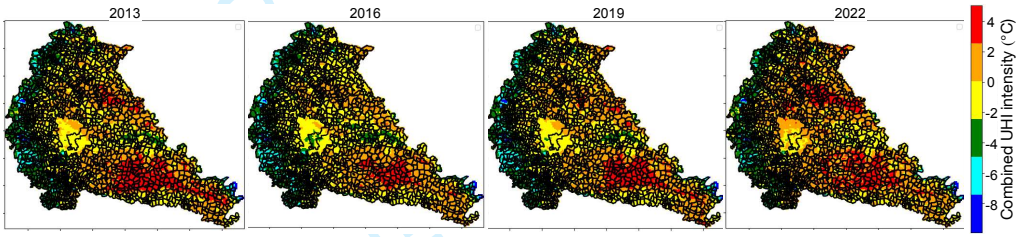


Figure 8.: Urban Hotspot Map of UHI (2013-2022)

*3.4.1. Identification of Urban Hotspots*

UHS were concentrated in Pune's western and central areas, characterized by limited vegetation and high-albedo surfaces. The highest UHI intensity was observed in 2022 (0.72°C), while the lowest was in 2016 (0.11°C). The spatial distribution of UHI and UHS, as depicted in Figure 8. Major UHS included parking lots, highways, industrial zones, and rooftops with minimal greenery or water bodies. Figure 8 shows the spatial distribution of UHS for 2013, 2016, 2019, and 2022, with a color gradient (blue to red) highlighting the progressive increase in hotspot intensity and spatial coverage, especially in central and southeastern regions, driven by urbanization and anthropogenic activities.

### 3.5. *Ecological Evaluation through UTFVI*

The UTFVI evaluates UHI ecological impacts index, categorizing thermal conditions into six indices (Figure 9a). From 2013 to 2016, areas in the "excellent" category (UTFVI $< 0$) remained stable in the southwest and northeast, while "poor" areas (UTFVI $> 0.020$) expanded, particularly along urbanized strips. Smaller patches exhibited "good" and "normal" conditions ($0 <$ UTFVI $< 0.02$), whereas "bad" and "worse" conditions were prevalent in built-up zones, indicating higher UHI intensity. Figure 9b further identifies UHI-prone areas based on UTFVI ranges, reflecting the ecological stress induced by urbanization.

### 3.6. $NO_2$ *Concentration*

| UTFVI | UHI | EEI. |
|---|---|---|
| $< 0.00$ | None | Excellent |
| 0.000–0.005 | Weak | Good |
| 0.005–0.010 | Moderate | Normal |
| 0.010–0.015 | Strong | Bad |
| 0.015–0.020 | Stronger | Worse |
| $> 0.020$ | Strongest | Worst |

(a)

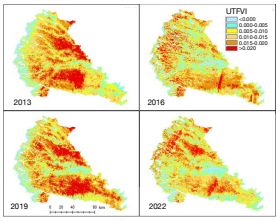


(b)

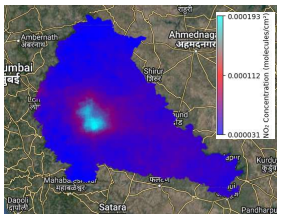


(c)

Figure 9.: (a) Classification of UTFVI with Corresponding UHI Intensity and Ecological Evaluation Index (EEI). (b) UTFVI-based ecological evaluation over the Study Years. (c) Gradient map highlighting $NO_2$ concentration over Pune.

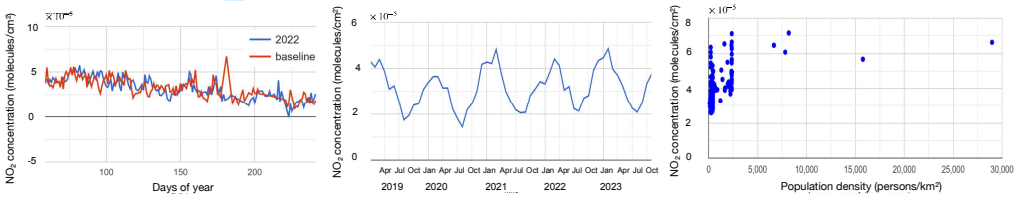


Figure 10.: (a) Comparison of $NO_2$ Concentration for baseline 2019 and 2022. (b) Monthly Mean $NO_2$ Concentration. (c) Scatter Plot of $NO_2$ vs Population Density.

The relationship between UHIs and atmospheric $NO_2$ concentrations, based on Sentinel-5P satellite data, reveals a statistically significant rise in $NO_2$ levels from the baseline year 2019 to 2022. The mean concentration increased from 0.000031 molecules/cm$^2$ in 2019 to 0.000036 molecules/cm$^2$ in 2022, with a maximum value of 0.000193 molecules/cm$^2$ recorded in 2022. While the visual differences in $NO_2$ trends may appear subtle in Figure 10a, the rise is supported by additional statistical analysis ($p$-value $< 0.05$) and verified by supplementary visualizations. To further explore this, Figure 10a illustrates the daily $NO_2$ concentrations (Day of Year) for March to August in 2019 and 2022, highlighting day-to-day variability and subtle differences in trends. Figure 10b presents the monthly mean $NO_2$ concentrations over multiple years (2020–2023), capturing seasonal and temporal variations that show higher concentrations in specific periods. Additionally, Figure 10c explores the correlation between $NO_2$ concentrations and population density. The scatter plot reveals the clustering of higher $NO_2$ levels in areas with greater population density, emphasizing the role of anthropogenic activities in driving these trends. This supports the observation that elevated $NO_2$ concentrations are often associated with urbanization and industrial activity, particularly in the central region of the area, as shown in Figure 9c.

## 4. Conclusion

The study on Pune's rising LST underscores growing concerns regarding urban health and environmental sustainability amid rapid urbanization and climate change. Using remote sensing data and the Urban Temperature-Adjusted Vegetation Index, the analysis highlights a significant rise in LST, with central urban areas experiencing heat while peripheral zones remain relatively cooler. These findings emphasize Pune's vulnerability to the Urban Heat Island effect, stressing the need for strategic urban

planning to maintain ecological balance and preserve green spaces. The study further highlights the importance of incorporating high-resolution data and ground-based monitoring for precise ecological assessments, aiding sustainable urban development.

## Data Availability Statement

Data sharing is not applicable – no new data is generated.

## References


Badugu, A., K. S. Arunab, A. Mathew, and P. Sarwesh (2023). Spatial and temporal analysis of urban heat island effect over tiruchirappalli city using geospatial techniques. *Geodesy and Geodynamics 14*(3), 275–291.

Bagyaraj, M., V. Senapathi, S. Karthikeyan, S. Chung, R. Khatibi, A. Nadiri, and B. Lajayer (2023). A study of urban heat island effects using remote sensing and gis techniques in kancheepuram, tamilnadu, india. *Urban Climate 51*, 101597.

Chauhan, S. and A. S. Jethoo (2023). Statistical analysis of diurnal variations in land surface temperature and the uhi effect using aqua and terra modis data. *Remote Sensing Letters 14*(5), 503–511.

Elmarakby, E. and H. Elkadi (2024). Impact of urban morphology on urban heat island in manchester's transit-oriented development. *Journal of Cleaner Production 434*, 140009.

Firozjaei, M. K., A. Sedighi, S. Kiavarz, S. Qureshi, D. Haase, and S. K. Alavipanah (2019). Automated built-up extraction index: A new technique for mapping surface built-up areas using landsat 8 oli imagery. *Remote Sensing 11*(17), 1966.

Guo, F., D. Hertel, U. Schlink, D. Hu, J. Qian, and W. Wu (2024). Remote sensing-based attribution of urban heat islands to the drivers of heat. *IEEE Transactions on Geoscience and Remote Sensing 62*, 1–12.

Harod, R. and E. Rajasekaran (2024). All-weather land surface temperature estimation by combining thermal infrared and passive microwave radiometry: A study over india. *International Journal of Remote Sensing 45*(18), 6691–6718.

Ialongo, I., H. Virta, H. Eskes, J. Hovila, and J. Douros (2020). Comparison of tropomi/sentinel-5 precursor no2 observations with ground-based measurements in helsinki. *Atmospheric Measurement Techniques 13*(1), 205–218.

Karutz, R., C. J. Klassert, and S. Kabisch (2023). On farmland and floodplains—modeling urban growth impacts based on global population scenarios in pune, india. *Land 12*(5), 1051.

Kowe, P. et al. (2022). Impacts of the spatial configuration of built-up areas and urban vegetation on land surface temperature using spectral and local spatial autocorrelation indices. *Remote Sensing Letters 13*(12), 1222–1235.

Mohammad, P. and A. Goswami (2022). Predicting the impacts of urban development on seasonal urban thermal environment in guwahati city, northeast india. *Building and Environment 226*, 109724.

Portela, C. I., K. G. Massi, T. Rodrigues, and E. Alcântara (2020). Impact of urban and industrial features on land surface temperature: Evidence from satellite thermal indices. *Sustainable Cities and Society 56*, 102100.

Wang, R., H. Hou, Y. Murayama, and A. Derdouri (2020). Spatiotemporal analysis of land use/cover patterns and their relationship with land surface temperature in nanjing, china. *Remote Sensing 12*(3), 440.

Wu, Q., Y. Huang, P. Irga, P. Kumar, W. Li, W. Wei, H. K. Shon, C. Lei, and J. L. Zhou (2024). Synergistic control of urban heat island and urban pollution island effects using green infrastructure. *Journal of Environmental Management 370*, 122985.